# Comparative analysis of internal energy excitation and dissociation of nitrogen predicted by independently developed *ab initio* potential energy surfaces

Maninder S. Grover, Paolo Valentini, Thomas E. Schwartzentruber, Richard L. Jaffe, Nicholas J. Bisek, and Ashley M. Verhoff

Phys. Rev. Fluids **7**, 123401 — Published 8 December 2022

DOI: 10.1103/PhysRevFluids.7.123401

# Comparative analysis of internal energy excitation and dissociation of nitrogen predicted by independently developed *ab initio* potential energy surfaces.

Maninder S. Grover * and Paolo Valentini †
*University of Dayton Research Institute, 1700 S Patterson Blvd, Dayton, OH 45469, USA.*

Thomas E. Schwartzentruber ‡
*Department of Aerospace Engineering and Mechanics, University of Minnesota, Minneapolis, MN 55455, USA.*

Richard L. Jaffe §
*NASA Ames Research Center, Moffett Field, California 94035, USA.*

Nicholas J. Bisek ¶ and Ashley M. Verhoff ‖
*Air Force Research Laboratory, Wright-Patterson Air Force Base, OH 45433, USA.*

**In this article we present a comparative atomic level study analyzing the vibrational excitation and dissociation of molecular nitrogen due to $N_2$ ($^1\Sigma_g^+$) + N ($^4S_u$) and $N_2$ ($^1\Sigma_g^+$) + $N_2$ ($^1\Sigma_g^+$) interactions governed by independently developed potential energy surfaces at the University of Minnesota and NASA Ames Research Center. Vibrational excitation was studied for $N_2$ + $N_2$ interactions from T = 10000 K to 25000 K and for $N_2$ + N from T = 5000 K to 30000 K. Nonequilibrium dissociation is studied from T = 10000 K to 30000 K under the quasi-steady state (QSS) condition for $N_2$ + $N_2$ and $N_2$ + N interactions. Lastly, an inviscid Mach 20 dissociating nitrogen flow over a cylinder with a Knudsen number of 0.015 is carried out to study the impact of molecular interactions predicted by independently developed potential energy surfaces on a canonical hypersonic flow.**

## I. Introduction

Strong shocks generated at the bow of reentry vehicles cause the gas temperature to rise to thousands of Kelvin. The post-shock heated gas experiences excitation of internal energy modes and chemical reactions. However, given the relatively low air density at high altitudes and the high speed of the flow, the rate of internal energy excitation and chemical reactions often competes with local characteristic flow times. This causes the gas enveloping the vehicle to be in thermal and chemical nonequilibrium [1]. The rate laws in computational fluid dynamics (CFD) solvers used

*Aerothermal Research Engineer, University of Dayton.
†Aerothermodynamic Research Engineer, University of Dayton.
‡Professor, University of Minnesota.
§Research Scientist, NASA Ames Research Center.
¶Senior Research Aerospace Engineer, AFRL/RQHF.
‖Research Aerospace Engineer, AFRL/RQHF.

to capture these phenomena are based on experimental data from the 1960s and 70s [2–4]. These rates often vary by orders of magnitude between different experimental datasets, as seen in Refs. [5–8], and need to be extrapolated to temperatures encountered in reentry flight. The base variance in the rate laws and their non-linear nature introduce significant uncertainty in CFD calculations.

In recent years there have been efforts to complement the experimental databases of thermochemical properties with high-fidelity data from computational chemistry. In this approach, an interaction potential is first generated for the particle interaction of interest. This is done by solving the electronic Schrödinger equation [9–15] to generate single point energies for thousands of geometries of the interaction of interest, then sophisticated fitting techniques, typically leveraging polynomial forms [9–15] or neural networks [16, 17], are used to generate a mathematically smooth potential energy surface (PES). PESs derived in this manner are often termed as 'First-Principle' or '*ab initio*' PESs. These PESs are then leveraged to calculate scattering trajectories [18, 19], aggregates of which are used to determine the thermochemical and kinetic properties.

A common method for using these scattering trajectories is the state-to-state (StS) method [20–23]. In this approach, a large number of trajectories calculations are performed at pre-determined conditions. These trajectories are then used to derive molecular internal energy state transition rates and state specific chemical reaction rates. A database of state transition rates is then incorporated into a flow solver that evaluates the master equation [20] and tracks each internal state as a pseudo-species in the flow [23–27]. These solvers are used to conduct 0-D reactor simulations [27–29] to determine thermochemical properties. Even though the StS method is a powerful approach, it can become intractable for molecule-molecule interactions. For example when all quantized ro-vibrational states are taken into account, there are of the order of $10^{15}$ possible state transitions for $N_2$ + $N_2$ interactions. To make StS simulations feasible for such systems, energy states are binned together [26, 27, 30–32]. However, it has been shown that binning of internal states leads to a loss of information about relaxation between internal states, which can cause variations in macroscopic thermochemical properties based on binning strategy [33]. Since the scattering trajectory calculations done using *ab inito* PESs are expensive, and have to be completed *a priori* to StS simulations this often translates to these simulations being run on sparsely populated dataset that may not have adequate resolution for every relevant state transition in a flow simulation. Thus, StS simulations have to interpolate between state transition rates which follow non-linear trends in the temperature range of interest. Furthermore, as the construction of the state transition database requires significant investment in running scattering trajectories, StS methods are more rigid to adapt to newer PESs, or to explore state transitions given by different PESs.

In this work we use the direct molecular simulation (DMS) [34] approach. Unlike the StS method [20] described above, DMS implements the scattering trajectory calculation within a time-accurate flow-field simulation. In this way the DMS method bypasses the need for binning energy states and is able to capture all statistically significant state transitions in a given simulation. Therefore, DMS simulations have no *a priori* assumptions and use the relevant PES(s)

as the only modeling input for the calculation. The ability to run scattering collisions on-the-fly also makes DMS an ideal tool to substitute different PESs for the same system to conduct a comparative study. In the past the DMS method has been used to calculate thermochemical properties in 0-D reactors [35–39], 1-D shock calculations [40], and recently has been expanded to study 2-D hypersonic flow [41–43], and transport properties [44]. In this study we consider independently developed PESs at the University of Minnesota [9, 10] and NASA Ames Research Center [11, 12] designed to capture high energy $N_2$ + $N_2$ and $N_2$ + N collisions using different computational chemistry techniques. The objective of this work is to compare thermochemical properties predicted by these PESs. This is achieved by:

1) Conducting 0D isothermal heat bath studies to calculate and compare characteristic vibrational excitation times.
2) Comparing nonequilibrium dissociation rate coefficients using a 0D reactor under quasi-steady state (QSS) conditions.
3) Comparing molecular level details such as the energy distribution functions predicted under nonequilibrium conditions.
4) Comparing flow field features due to a Mach 20 dissociating nitrogen flow over a 2D cylinder.

## II. Direct Molecular Simulation

### A. Method Overview

Detailed description of the DMS method can be found in Ref. [34] this section only provides a brief overview for clarity. The DMS method is a high-fidelity variant of the Direct Simulation Monte Carlo (DSMC) method of Bird [45]. Similar to DSMC, the DMS is a particle method that predicts flow characteristics by aggregating particle properties in a simulation cell. The simulation time-steps are of the oder of the mean collision time ($\tau_c$), the simulation cell sizes are of the order of the local mean free path ($\lambda_c$), and the ratio of the actual particles to the simulated particles in the control volume is called the particle weight ($W_p$). Every time-step a representative number of particles in the simulation domain are selected to undergo collisions to approximate the mean collision rate of the gas. However, where the standard DSMC approach uses stochastic collision models, the DMS method carries out scattering trajectory calculations using the appropriate PES [19, 34] to determine the collision outcome.

When a particle pair is selected for trajectory integration, the phase-space coordinates of all atoms of the colliding particles are integrated using a velocity Verlet scheme [46]. The time-step for trajectory integration is set to $\Delta t_{traj}$ = 0.05 fs. The trajectory is integrated until the minimum separation between the atoms not bounded to the same molecule is greater than the minimum cut-off distance $D_0$ = 15 Å. During a trajectory, for certain atomic configurations, the atoms may go over local free energy maxima in the PES. This may lead to the formation of new bonds and breaking of others. Hence, the DMS method automatically accounts for all collision outcomes available in the PES. After the trajectory integration is completed, each molecule is analyzed to establish if it is bound, quasi-bound, or dissociated. Then as a

post-processing step the internal energy of the molecule is calculated using the position and velocity of the bound atoms. Currently, the DMS method does not allow for recombination of atomic species back to molecules as research is actively being conducted in the proper treatment of three body collisions and recombination for scattering trajectories [47, 48].

The 0D reactor simulations discussed in Sec. III are obtained using an in-house DMS code developed at the University of Minnesota, and the 2D simulations shown in Sec. IV are obtained by incorporating DMS routines in the Stochastic PArallel Rarefied-gas Time-accurage Analyzer (SPARTA) DSMC code developed at Sandia National Laboratories [49]. Details for this implementation are discussed in Ref. [41, 42].

### B. Potential Energy Surfaces

This section provides a high-level overview of the PESs used in this study. A PES is a fit to the potential energy of various atomic arrangements of the interacting system. The gradients of the PES is used to perform the molecular trajectory calculation as discussed in Sec. II.A and the PESs serve as the only modeling input to the DMS method. Early attempts at defining PESs were based on a combination of theoretical calculations and empirical data from experiments [50–55]. These PESs are often represented with simple analytical functions. However, due to the simplicity of the fitting functions, and use of inadequate data to resolve atomic interactions [56], such PESs are less accurate for modeling molecular interactions involving high collision energy. In recent years, PESs tailored to capture high energy interactions have been produced [9–15]. These potential energy surfaces are derived from extensive quantum mechanical calculations, where the electronic Schrödinger equation is solved to give the potential energy of the interacting nuclei. These PESs derived from first principles are called *ab initio* PESs. In this work we use *ab initio* PES developed at the University of Minnesota and NASA Ames Research Center.

The group at NASA Ames Research Center developed separate PESs for $N_2$ + $N_2$ interactions (NASA $N_4$ PES) and $N_2$ + N interactions (NASA $N_3$ PES). The details of the NASA PESs can be found in Refs. [11, 12, 56]. Broadly, both NASA PESs use an augmented correlation consistent polarized valence triple zeta (aug-cc-pVTZ) [[57, 58] basis set. The aug-cc-pVTZ basis set contains five s-orbitals, four p-orbitals, three d-orbitals and two f-orbitals for each atom. The NASA PESs utilize two different methods to compute electron correlation. The coupled cluster method - CCSD(T) [59] was used for geometries where two distinct nitrogen molecules exist. For other geometries the multi-reference configuration interaction (MRCI) [60] method is used with complete active space self-consistent field (CASSCF) [61] molecular orbitals. The NASA $N_4$ PES has 4146 single energy points, with 3821 points obtained from CCSD(T) and 325 points from CASSCF-MRCI. The NASA $N_3$ PES has 3885 single energy points calculated using CCSD(T). Additionally, both NASA PESs use the diatomic potential energy function proposed by Le Roy *et al.* [62] to describe the $N_2$ diatom.

The PES developed at the University of Minnesota (UMN PES) [9, 10] uses a minimally augmented correlation consistent polarized valence triple zeta (maug-cc-pVTZ) basis set [63]. This maug-cc-pVTZ formulation is similar to

the aug-cc-pVTZ formulation discussed above but ignores some d-orbitals and f-orbitals from the augmentation set [63]. The PES also uses complete active space SCF [61] used to obtain molecular orbitals. The UMN group uses a second order perturbation method CASPT2 [64–66] to obtain all single point energies. The UMN PES has a total of 16547 single point energies, out of which 1,017 were calculated for the $N_2$ + N system. As such, this PES is able to resolve both: $N_2$ + $N_2$ and $N_2$ + N interactions [36]. The properties of diatomic $N_2$ as given by these PESs are shown in Table 1. The differences in the numbers of bound and quasibound levels between UMN and NASA PESs are mainly due to small differences in the long-range nature of the diatomic potentials.

| Quantity | UMN PES | NASA PES |
|---|---|---|
| Dissociation energy at j=0 | 9.91 eV | 9.89 eV |
| Number of vibrational levels for j=0 | 55 | 61 |
| Number of rotational levels for v=0 | 279 | 279 |
| Number of ro-vibrational levels | 9198 | 9390 |
| Number of bound ro-vibrational levels | 7122 | 7421 |
| Number of quasi-bound ro-vibrational levels | 2076 | 1969 |

**Table 1 Properties of diatomic nitrogen from the potential energy surfaces developed at the University of Minnesota [9, 10] and NASA Ames Research Center [11, 12].**

### C. Treatment of Internal Energy

The DMS method operates on atomic positions and velocities. For atoms bound in a molecule, atomic positions and velocities may be post processed to obtained the ro-vibrational internal energy of the molecule [34]. Therefore, DMS calculations do not assume any *a priori* decoupling between rotational vibrational modes. To divide the internal energy into rotational and vibrational modes, the vibrational prioritization framework as discussed in Ref. [67] is used. In this framework, the internal ro-vibrational energy ($\varepsilon_{int}(v, j)$) is used to calculate the vibrational ('$v$') and rotational ('$j$') level of the molecule. Then the molecule is first assigned the vibrational energy of level '$v$' corresponding to rotational level $j = 0$ :

$$\varepsilon_{vib}(v) = \varepsilon_{int}(v, 0) \ . \tag{1}$$

The remaining internal energy is assigned to the rotational mode.

$$\varepsilon_{rot}(j) = \varepsilon_{int}(v, j) - \varepsilon_{int}(v, 0). \tag{2}$$

To characterize macroscopic evolution of the rotational mode in this article, rotational temperature is defined as the average rotational energy normalized by Boltzmann's constant.

$$T_r = \frac{\langle \varepsilon_{rot} \rangle}{k_B} \ . \tag{3}$$

Similarly, in this article the average energy in the vibrational mode is used to define vibrational temperature as :

$$T_v = \frac{\langle \varepsilon_{vib} \rangle}{k_B} \ . \tag{4}$$

## III. Thermochemical Properties

### A. 0-D Isothermal Reactor

Isothermal 0-D reactor simulations are used to study and compare characteristic vibrational excitation (Sec. III.B) and nonequilibrium dissociation (Sec. III.B) due to $N_2$ + $N_2$ ($N_4$) and $N_2$ + N ($N_3$) interactions separately. Then 0-D isothermal reactors are used to assess the behavior of a system characterized by both $N_4$ and $N_3$ interactions. For the isothermal simulations presented in this section, the desired temperature is maintained by sampling particle center of mass velocities from a corresponding Maxwell-Boltzmann distribution, and a density is set to $\rho$ = 1.28 kg/m$^3$.

Figure 1 shows the time dependent composition and temperature profiles of an isothermal 0-D DMS calculation at T = 30000 K. In this example, the gas is initialized such that at t = 0 $\mu$s the translational (blue), rotational (black) and vibrational (red) temperatures are in equilibrium : $T_t = T_r = T_v$ = 30000 K. As the system evolves dissociation results in the decrease in the mass fraction of molecular nitrogen (purple) and an increase in mass fraction of atomic nitrogen (green). Due to dissociation, the population of molecules with higher rotational and vibrational energy is depleted. As seen in Fig. 1, this causes the average rotational and vibrational energies to decrease from the equilibrium value at t > 0. As the inelastic collisions and exchange reactions [36, 68] re-populate the higher energy states, a new balance is achieved between re-population and depletion of higher internal energy levels. This balanced state is termed the Quasi-Steady State (QSS), and is characterized by time invariant internal energy distributions and stabilization of average internal energies. It can be seen in Fig. 1 that this system reaches QSS around t = 0.001 $\mu$s.

Figure 2(a) shows the Boltzmann and QSS vibrational energy distribution at T = 30000 K. It can be seen that the QSS vibrational energy distribution is non-Boltzmann and has a depleted population at the higher vibrational energy levels when compared to the corresponding Boltzmann distribution. Similarly, Fig. 2(b) shows the Boltzmann and QSS rotational energy distribution. The QSS rotational distribution is non-Boltzmann and has depleted populations at the higher rotational levels. The QSS is a consequence of re-population of high energy states by inelastic collisions and depletion due to collisions that result in dissociation, so the QSS depends only on the local collision rate. In other words, the QSS is uniquely defined for a given temperature and density of the gas and is independent of the initial internal energy state of the isothermal reactor. This conclusion is illustrated by Fig. 2(c). In the figure, the translational temperature (blue) is held constant at $T_t$ = 30000 K, and then the rotational (black) and vibrational (red) temperatures are

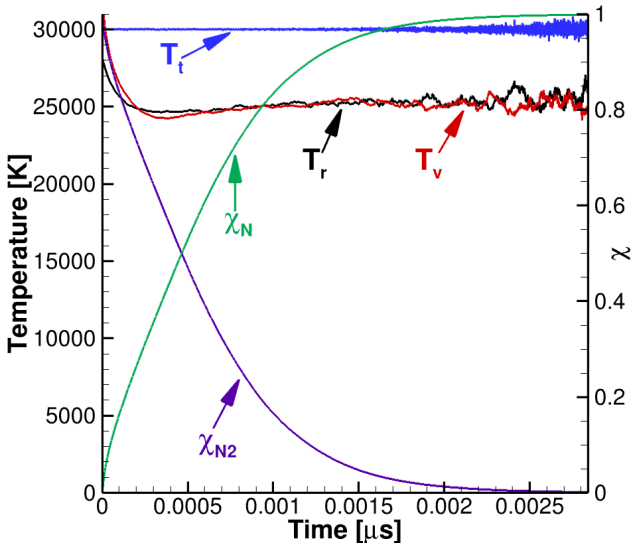


**Figure 1 Example of isothermal relaxation in a box and formation of the QSS for the full nitrogen system (both $N_2$ + $N_2$ and $N_2$ + N interactions allowed) using the NASA Ames PESs. [11, 12]**

initialized at $T_r = T_v$ = 30000 K, 15000 K, and 3000 K. It can be seen that regardless of the initial internal temperature that is assigned to the gas, the systems stabilizes to the same QSS.

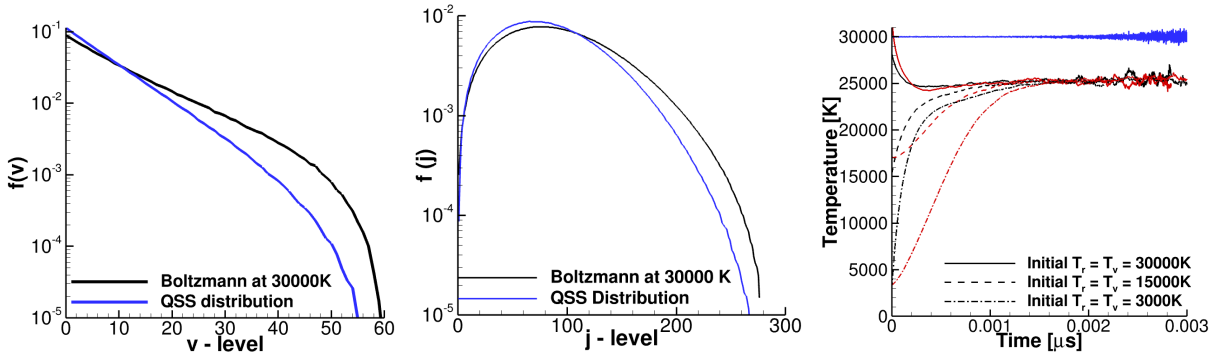


(a) Vibrational Energy Distribution in QSS. (b) Rotational Energy Distribution in QSS. (c) QSS for various initial internal energy states of the gas.

**Figure 2 Characteristics of QSS at T = 30000 K.**

### B. Characteristic Vibrational Excitation Time

Characteristic vibrational excitation times are derived by conducting 0D isothermal relaxation calculations as described above. The temporal profiles of the average vibrational energy are fit to the solution of a first order ordinary differential equation (ODE):

$$\frac{\mathrm{d}\langle \varepsilon_{vib}(t)\rangle}{\mathrm{d}t} = \frac{\langle \varepsilon^{*}_{vib}\rangle - \langle \varepsilon_{vib}(t)\rangle}{\tau_{vib}} \tag{5}$$

to determine $\tau_{vib}$. Here $\langle \varepsilon_{vib}(t) \rangle$ is the instantaneous value of the average vibrational energy and $\langle \varepsilon^*_{vib} \rangle$ is the average vibrational energy under equilibrium conditions.

To calculate the characteristic vibrational excitation time due to $N_2$ + $N_2$ interactions ($\tau_{vib}^{N_2+N_2}$ ), $N_2$ + N interactions are excluded in the heat bath calculations. The results of these calculations are shown in Fig. 3. The DMS calculations using the NASA $N_3$ PES (blue square symbols with solid line) and the UMN PES (red triangle symbols with solid line) produce qualitatively similar results, with the maximum variation between $\tau_{vib}^{N_2+N_2}$ predicted by the two PESs being about $\sim$ 16 % at 10000 K. The difference in the predicted $\tau_{vib}^{N_2+N_2}$ decreases with an increase in temperature. Furthermore, it is observed that the DMS results for $\tau_{vib}^{N_2+N_2}$ match closely with the Millikan and White fit [2, 69] (solid black line) for the characteristic vibrational excitation time. However, while the high temperature correction of Park [2] causes the characteristic excitation time to increase past 20000 K the DMS calculations show that the characteristic excitation time keeps decreasing.

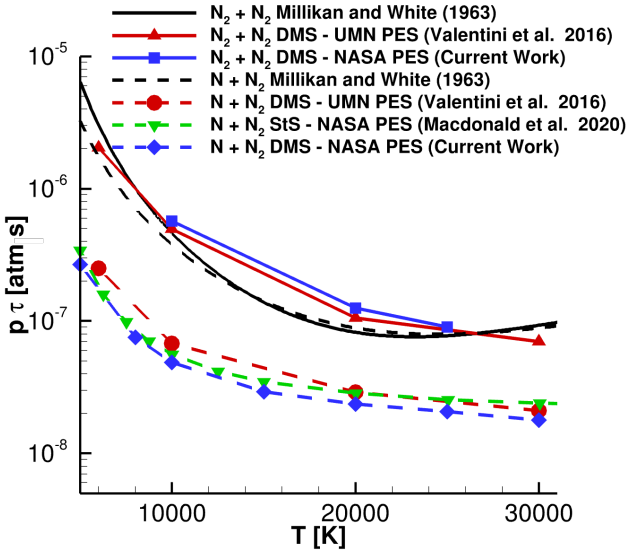


**Figure 3 Characteristic vibrational excitation times for $N_2$ + $N_2$ and $N_2$ + N interactions.**

To calculate characteristic vibrational excitation time due to $N_2$ + N interactions ($\tau_{vib}^{N_2+N}$ ), 0D isothermal excitation calculations are carried out for a mixture of $N_2$ and N where the partial density of molecular nitrogen is initialized at $\rho_{N_2}/\rho = 0.01$. The DMS calculations using the NASA $N_3$ PES (blue diamond symbols with dashed line) and the UMN PES (red circle symbols with dashed line) are seen to produce qualitatively similar results, with the maximum variation between the predicted $\tau_{vib}^{N_2+N}$ from the two PESs is about $\sim$ 28 % at 10000 K, with the difference in $\tau_{vib}^{N_2+N}$ decreasing with an increase in temperature. When comparing the StS calculations of Macdonald *et al.* [70] (green inverted triangles with dashed line) we see excellent agreement for the predicted $\tau_{vib}^{N_2+N}$ at lower temperatures. The difference between the predicted $\tau_{vib}^{N_2+N}$ values increases with increase in temperature resulting in a maximum difference of $\sim$ 33 % at the maximum calculated temperature of 30000 K. Note that Macdonald *et al.* [70] used the same NASA

$N_3$ PES as this work, therefore, difference in the results is due to the numerical approach. Lastly, when compared to the Millikan and White fit [69], it can be seen that all computational chemistry results are approximately an order of magnitude lower. This faster excitation due to $N_2$ + N interactions has been attributed to exchange reactions which have been shown to be more efficient in redistributing vibrational energy [36, 68].

### C. Nonequilibrium Dissociation

In this section we discuss dissociation under QSS conditions. As discussed above, QSS represents a balance between depletion and re-population of high energy levels and therefore provides a metric to compare the two kinds of molecular interactions on the PESs concurrently. A comparative analysis of dissociation under QSS purely due to $N_2$ + $N_2$ interactions given by the NASA and UMN PESs has been discussed in Ref. [56]. In this work, we extend that analysis to $N_2$ + N interactions and to the combined system where $N_2$ + N and $N_2$ + $N_2$ interactions can occur simultaneously.

#### *1. $N_2$ + N Interactions*

In this section we discuss dissociation due to $N_2$ + N collisions. As described in the previous section (Sec:III.B in order to isolate the effects of atom-molecule collisions in DMS, isothermal 0D calculations were conducted for a mixture of nitrogen atoms and molecules where the partial density of molecular nitrogen is reduced to $\rho_{N_2}/\rho = 0.01$. The heat bath is then simulated until the system is in QSS. Once the system is in QSS the dissociation rate coefficient is calculated by fitting the temporal composition profile to the following equation:

$$\frac{d[N_2]}{dt} = -k_d^{N_2+N_2}[N_2]^2 - k_d^{N+N_2}[N][N_2] \ . \tag{6}$$

Since $[N_2] << [N]$ the first term in Eq. 6 is ignored and we assume that $[N]$ does not change in time because, at $t = 0$, $[N] >> [N_2]$. Therefore, $[N](t) \sim [N](t = 0) = [N]_0$. This reduces Eq:6 to a pseudo-first order rate law given by:

$$\frac{d[N_2]}{dt} = -[N]_0 k_d^{N+N_2}[N_2] \ . \tag{7}$$

Figure 4(a) shows the QSS dissociation rate coefficients obtained from the above analysis. As seen, the dissociation rate coefficient in QSS, purely due to $N_2$ + N interactions ($k_{d|QSS}^{N_2+N}$) predicted by the NASA PES (blue diamond symbols with solid line) is nearly 50% higher than $k_{d|QSS}^{N_2+N}$ predicted by the UMN PES (red circular symbols with solid line) at T = 10000 K. However this difference decreases with increasing temperature such that the difference is only 10% at T = 30000 K. Additionally, we provide a comparison of dissociation rate coefficients in QSS for systems where only $N_2$ + $N_2$ interactions were allowed. This data was first published in Ref. [56] and since then more statistics have been collected for the QSS dissociation rate coefficient at 10000 K and an additional point of comparison has been added at

15000 K. The QSS dissociation rate coefficient for $N_2$ + $N_2$ interactions ($k_{d|QSS}^{N_2+N_2}$) is 50 % higher at 10000 K for the simulation using the NASA PES (blue square symbols with dashed lines) when compared to the simulation using the UMN PES (red triangular symbols with dashed line). The difference in predicted ($k_{d|QSS}^{N_2+N_2}$) decreases with increase in temperature, and the at 30000 K the nonequilibrium dissociation rate coefficient differs by 4%.

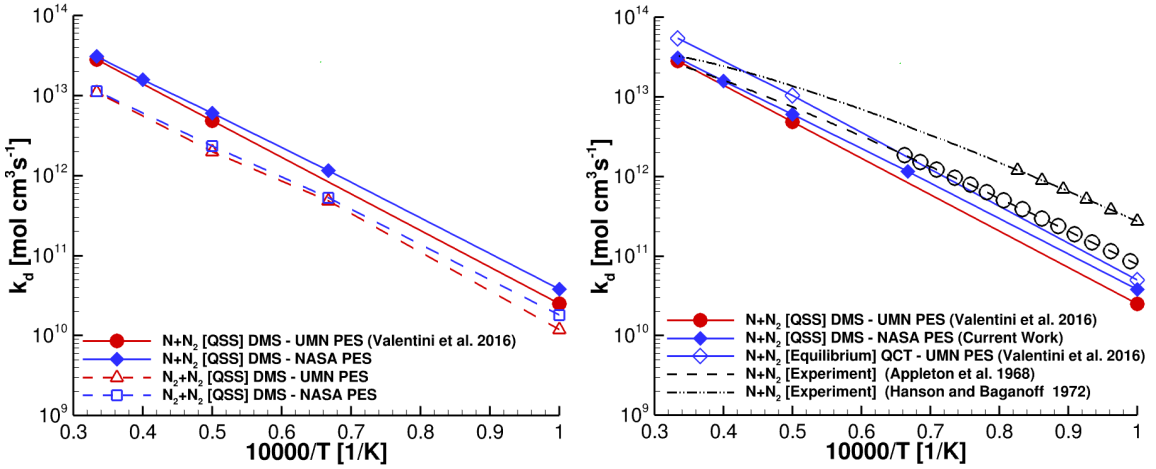


(a) Dissociation rate coefficients in QSS given by DMS.

(b) Comparison of DMS based dissociation rate coefficients and experimental and equilibrium data.

**Figure 4 Dissociation rate coefficients.**

Figure 4(a) also shows that the QSS dissociation rate for $N_2$ + N interactions is higher than that for $N_2$ + $N_2$ interactions. This can be explained using Fig. 5, which shows the vibrational distribution function in QSS. It can be seen at 30000 K (Fig. 5(a)), 20000 K (Fig. 5(b)), and marginally at 10000 K (Fig. 5(c)), that the QSS vibrational energy distribution is less depleted for the simulations that include $N_2$ + N dynamics. This higher population of vibrationally excited molecules is attributed to faster vibrational relaxation due to $N_2$ + N interactions as shown in Sec. III.B. Additionally, it can be seen that the vibrational energy distribution in QSS of simulations using the NASA PESs and the UMN PES agree well.

Figure 4(b) compares QSS dissociation rate coefficients with dissociation rate coefficients for $N_2$ + N in equilibrium [36]. It can be seen that the dissociation rate coefficients under equilibrium are higher than the QSS rate coefficients, this can be attributed to the QSS energy distributions being depleted at higher energy levels - as seen in Fig. 5. Additionally, Fig. 4(b) shows experimental data of Appleton *et al.* [7] and Hanson and Baganof [8]. The symbols on the experimental data show the temperature range for which the experiments were conducted. It can be seen that the variation between the experimental dissociation rate coefficients is larger than the difference in rate coefficients predicted from computational chemistry by the two PESs. Furthermore, as seen in Fig. 5 the vibrational energy distribution predicted by the two PESs in QSS is almost identical. This shows that at the atomistic level the two PESs predict similar rates of depletion and repopulation of the high energy tail of the vibrational energy distribution.

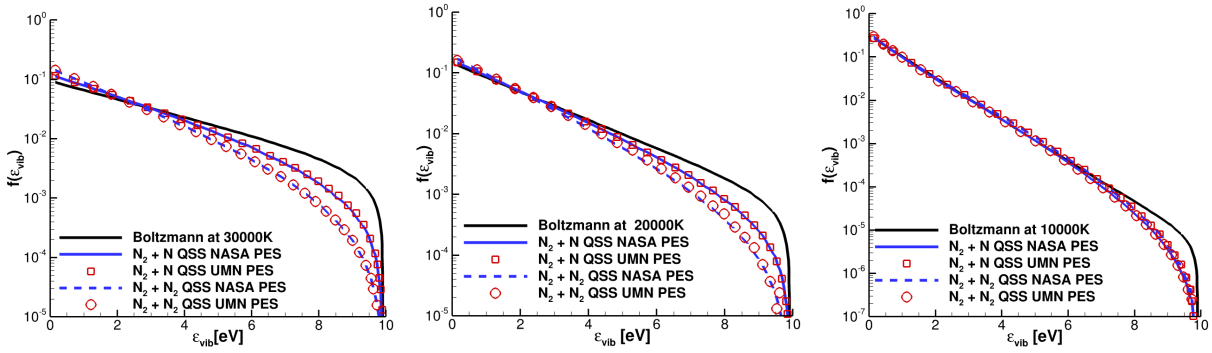


(a) 30000 K. (b) 20000 K. (c) 10000 K.

**Figure 5 QSS vibrational distribution functions for 0D systems where only $N_2$ + N or only $N_2$ + $N_2$ interactions where allowed.**

*2. $N_2 + N_2$ and $N_2 + N$ Interactions*

While the above sections have individually established the characteristics of $N_2$ + N and $N_2$ + $N_2$ interactions, in this section we study the behavior of isothermal heat baths that allow for both interactions to occur concurrently. Figure 6 show the time-evolution of temperature and composition in 0-D heat baths at 30000 K (Fig. 6(a)), 20000 K (Fig. 6(b)) and 10000 K (Fig. 6(c)). The plots show the translational temperature (blue), rotational temperature (black), vibrational temperature (red), and the mass fraction of atomic nitrogen (green). All three cases are initialized with pure molecular nitrogen in the reactor at t = 0 $\mu$s. The heat baths at 30000 K and 20000 K show excitation of internal temperatures from 3000 K to a QSS state, whereas the heat bath at 10000 K shows relaxation to QSS from an equilibrium state at T = 10000 K . These simulations show that the particle interactions predicted by the NASA PESs and UMN PES show a similar excitation rate for internal temperatures, however, the simulations using the NASA PESs allow for faster dissociation of molecular nitrogen.

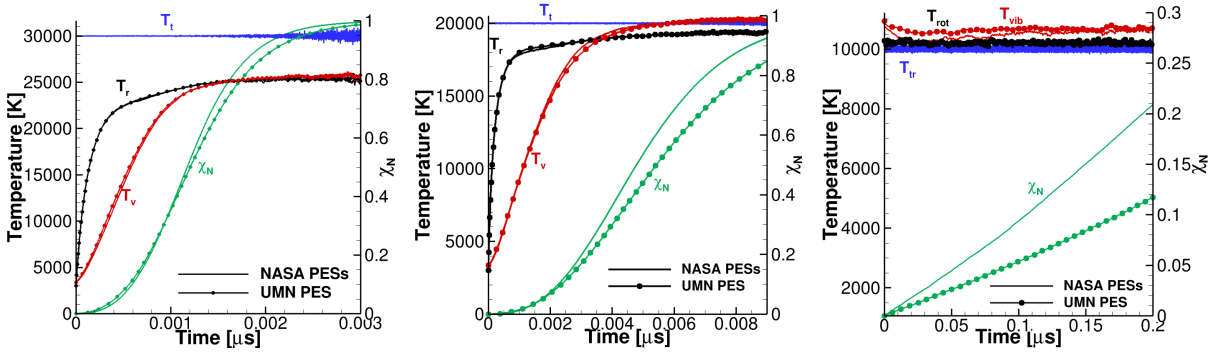


(a) $T_t$ = 30000 K. (b) $T_t$ = 20000 K. (c) $T_t$ = 10000 K.

**Figure 6 Composition and temperature history comparison of simulations including both $N_2$ + N and $N_2$ + $N_2$ interactions using the NASA PESs and the UMN PES.**

Figure 7 shows the vibrational distribution function during the QSS for the simulations shown in Fig. 6. It can

be seen that the two PESs predict similar QSS vibrational energy distributions. This shows that the faster vibrational excitation for simulations using the NASA Ames PES (as seen in Sec. III.B) facilitates the higher dissociation rates in simulations using the NASA Ames PES, while maintaining similar depleted distributions in the QSS.

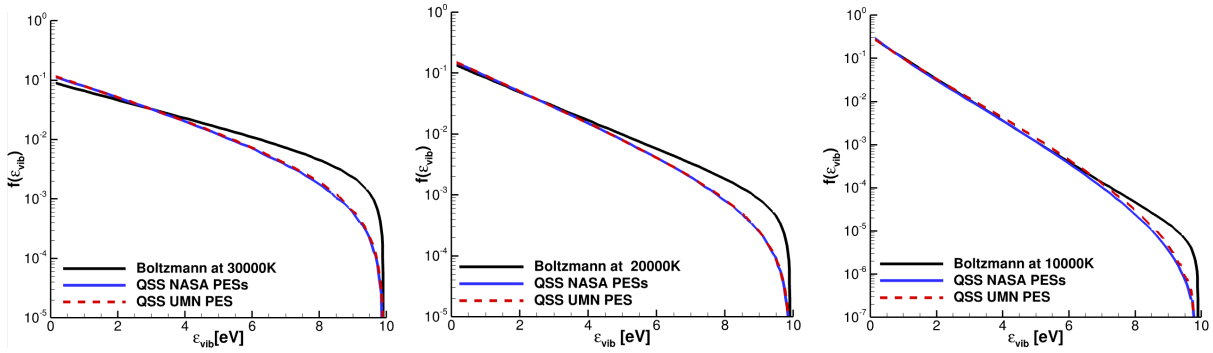


(a) $T_t$ = 30000 K. (b) $T_t$ = 20000 K. (c) $T_t$ = 10000 K.

**Figure 7 Vibrational energy distribution of $N_2$ molecules in QSS for simulation including both $N_2$ + N and $N_2$ + $N_2$ interactions.**

## IV. Hypersonic Dissociating Nitrogen Flow Past Cylinder

Recently, the DMS method has been expanded to perform 2-D fluid flow simulations [41–43]. As the $N_3$ and $N_4$ PESs are designed to resolve high energy collisions and are being used to develop thermochemical models for hypersonic flight [71, 72], comparing the flow fields given by two independently developed sets of PESs provides an unique opportunity to compare thermochemical characteristics predicted by PESs in an applied fluid dynamics scenario. In this section we discuss results comparing a Mach 20 dissociating nitrogen flow over a cylinder predicted by the NASA PESs and the UMN PES. We have used this case in the past to compare thermochemical characteristics of the UMN PES [9, 10] to an updated version [73] of the UMN PES where the single point energy data base was expanded from 16547 to 21406 single point energy points [42, 73]. It was concluded that the original UMN PES [9, 10] is sufficiently resolved and adding new single energy points for the data set did not meaningfully alter the solution [42]. While the *new* UMN PES compared in Ref. [42] was an improvement on the original and used the same quantum methods, the NASA PES provides a point of comparison outside of the UMN dataset and uses different quantum methods (discussed in Sec. II.B).

### A. Simulation Set Up

For the Mach 20 dissociating flow simulations the free stream density is set to $\rho_0 = 0.0184$ kg/m$^3$ and temperature T = $T_t$ = $T_r$ = $T_v$ = 226 K which corresponds to nominal conditions at 30 km with a free stream velocity u = 6130 m/s. The cylinder diameter $D_c$ = 0.2 mm and the cylinder surface is assumed to be adiabatic, *i.e.* all particles colliding with the wall are specularly reflected and there is no thermal or inertial accommodation at the cylinder surface. The Knudsen number based on the free stream is $K_n \approx 0.015$ which is in the range where Navier-Stokes solution (CFD) should also be

valid.

The grid is refined and coarsened in a manner the enforces the local grid size $\Delta x < 1.2\ \lambda_l$, where $\lambda_l$ is the local mean free path. A further refinement is done to the cells in the stagnation region such that $\Delta x < 0.6 \times \lambda_l$ to provide high resolution of the bow shock. The DMS time step is $\Delta t_{DMS} = 5 \times 10^{-11}$ s.

### B. Thermochemistry in the Flow Field

Figure 8 shows the translational (Fig. 8(a)), rotational 8(b), and vibrational 8(c) temperatures and the mass fraction of atomic nitrogen (Fig. 8(d)), from the 2D DMS calculations of Mach 20 flow over cylinder. The top half of the images show the flow field obtained using the UMN PES [9, 10] , and the bottom half shows the flow field obtained by using the NASA PESs [11, 12]. Figure 8(a) shows that the two PESs predict similar translational temperature fields and predict the same shock stand-off distance. From Fig. 8(b) one can see that both simulations predict similar rotational temperature profiles, with the simulation using the NASA PESs rotationally de-exciting slightly faster in the expansion region (x/D > 2.5). Figure 8(c) shows the vibrational temperature field predicted by the two simulations is comparable in the compression region (x/D < 2.5) but the simulation using the NASA PESs is vibrationally hotter in the expansion region (x/D > 2.5).

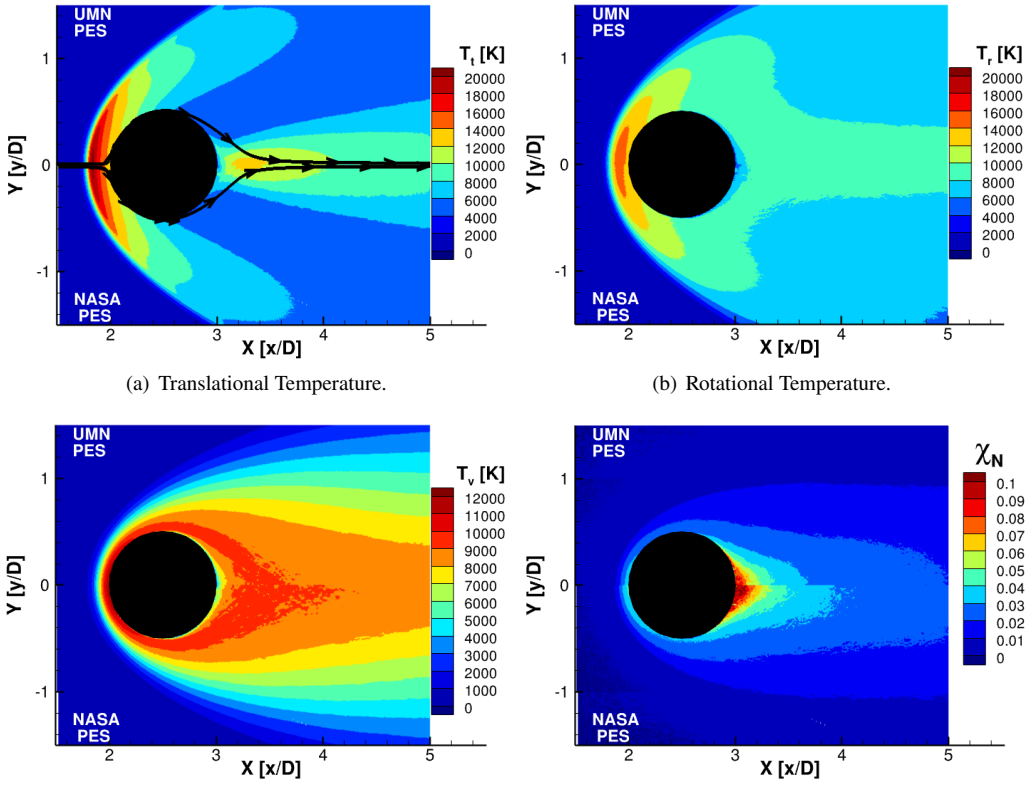


(a) Translational Temperature.

(b) Rotational Temperature.

(c) Vibrational Temperature.

(d) Mass Fraction of Atomic Nitrogen.

**Figure 8 Temperatures and composition of the Mach 20 flow field.**

Figure 8(d) shows the mass fraction of atomic nitrogen in the simulation using the NASA PES is higher than for the simulation using the UMN PES. The results also show that most of the production of the atomic nitrogen occurs in the stagnation region, however, the cylinder wake has the highest mass fraction of the atomic nitrogen. Recall that no recombination reactions are included in these DMS calculations.

Figure 9(a) shows the variation of translational (blue), rotational (black), and vibrational (red) temperatures along the streamlines included in Fig. 8(a). It can be seen that all three energy modes are excited across the bow shock. The translational and rotational modes quickly equilibrate behind the shock, whereas the vibrational mode is only partially excited. As the flow travels over the cylinder and, subsequently expands, there is a consistent drop in translational temperature while the rotational and vibrational modes freeze in a state of thermal nonequilibrium because the relaxation time for these modes is on the same order as the flow time scales. In the cylinder wake there is a peak in translational temperature associated with the closing of the streamlines behind the cylinder. However, the translation temperature relaxes towards thermal equilibrium as the flow accelerates behind the cylinder, while the rotational and vibrational modes continue to remain essentially frozen in this regime.

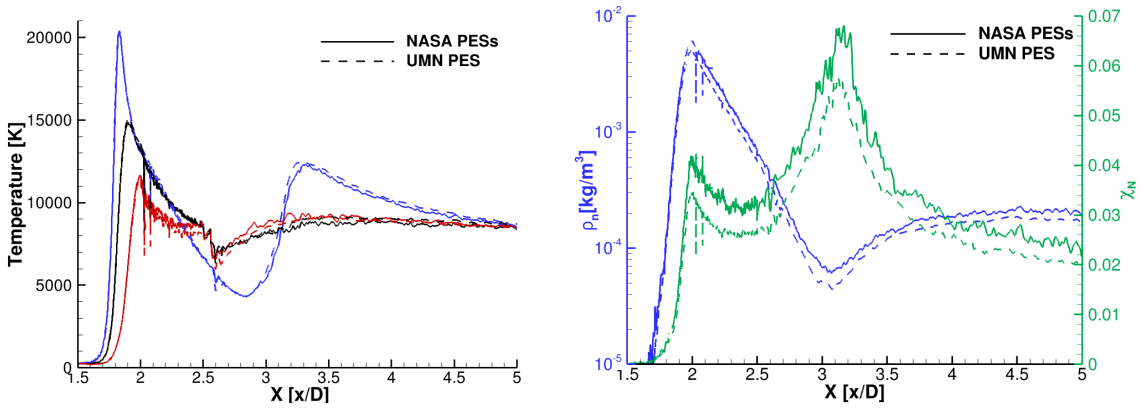


(a) Temperatures.

(b) Atomic Nitrogen Mass Fraction and Partial Density.

**Figure 9 Temperatures and composition along streamlines shown.**

Figure 9(b) shows the partial density of atomic nitrogen (blue) and the mass fraction (green) along the same streamlines. It can be seen that both partial density and mass fraction of atomic nitrogen increase behind the shock as molecular nitrogen dissociates in the compression region (1.5 < x/D < 2). Following the profile downstream between 2 < x/D < 3, there is a drop in partial density that is attributed to the decrease in total density due to expansion. As the stream line closes around x/D ~ 3.25 the partial density starts increasing again. Meanwhile, the mass fraction of atomic nitrogen drops between 2 < x/D < 2.5 due to volumetric expansion of the fluid. Between 2.5 < x/D < 3.5 a peak in the mass fraction of atomic nitrogen is observed. This peak is attributed to the high translational temperatures in this region and the low fluid velocity that promotes dissociation in the rarefied region behind the cylinder. As the fluid expands further downstream we see a drop in mass fraction of atomic nitrogen due to continued flow expansion and relaxation

back towards equilibrium.

### C. Stagnation Region

Figure 10(a) shows the temperatures and composition along the stagnation streamline. It can be seen that both simulations give the same shock stand-off distance for the translational temperature. The translation and rotational modes excite and equilibrate behind the shock, whereas the vibrational mode only partially excites behind the shock. As can be seen at the wall (x/D = 2), the trans-rotational temperature for the simulation using the UMN PES is slightly higher than the simulation using the NASA PESs. This can be attributed to a lower level of dissociation in the UMN PES simulation. This difference in the degree of dissociation results in a stagnation point mass fraction of atomic nitrogen of 0.034 for the UMN PES simulation and 0.042 for the simulation that used the NASA PESs. This corresponds to a difference of over 23% in atomic mass fraction which could have additional implications for non-specular surfaces.

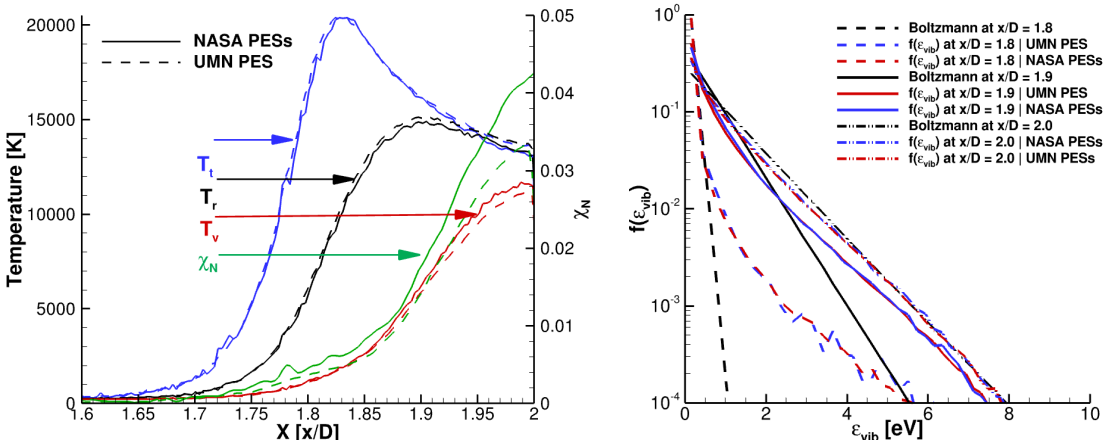


(a) Temperatures and Composition.

(b) Vibrational Distribution Functions.

**Figure 10 Temperature, composition, and vibrational distribution functions along stagnation streamline.**

Figure 10(b) shows the vibrational energy distribution along the stagnation stream line at selected points : x/D = 1.8 (dashed line) , 1.9 (solid line), 2.0 (dash-dot line). It can be seen that the energy distribution functions predicted by the two simulations using different PESs are virtually identical at all three points. At x/D = 1.8 the population in the low vibrational levels is populated in a manner similar to a Boltzmann distribution corresponding to this temperature, but the mid and high energy levels are overpopulated when compared to the corresponding Boltzmann distribution, resulting in a highly non-Boltzmann distribution. At x/D = 1.9 we see a deviation from Boltzmann behavior at both low and high vibrational levels. At x/D = 2.0, vibrational energy distributions still deviate slightly from Boltzmann behavior. This indicates that the vibrational excitation process, between the shock front (x/D = 1.8) and the stagnation point (x/D = 2.0) has a non-Boltzmann nature for this type of flow.

### D. Cylinder Flank

Figure 11(a) shows the temperature and composition profiles normal to the cylinder surface at the flank (x/D = 2.5). It can be seen that the translational temperature profile (blue) has two peaks. The first peak at y/D = 1.2 is due to the sampling line intersecting the oblique shock at x/D = 2.5. The second, broader peak around y/D = 0.8 is due to advection of shock heated gas from the stagnation region. At y/D < 0.8 a decrease in translational temperature is observed as the flow expands along the cylinder. Figure 11(a) also shows the rotational temperature (black) along this wall normal. It can be seen that the region is in rotational nonequilibrium, $T_r > T_t$ for y/D < 1.0. Here the rate of molecular interactions that equilibrate translational and rotational modes is slower than the rate at which the translational temperature cools due to expansion of the flow. A similar trend is observed for the vibrational mode.

Additionally, the solutions obtained using the NASA PESs (solid line) and the UMN PES (dashed line) are qualitatively similar along this sampling profile. There are some quantitative differences starting y/D ≈ 1 where the rotational mode for the simulation using the UMN PES is hotter than the simulation using the NASA PESs. Conversely, in this region, the simulation using the NASA PES is vibrationally hotter. Interestingly, results yielded by the NASA PESs are in rotational-vibrational equilibrium near the cylinder surface. This is not seen with the UMN PES and shows that the simulations using the NASA PESs have faster internal energy relaxation. Additionally, the system has a higher mass fraction of atomic nitrogen for the simulation using the NASA PESs, which is consistent with the observations made in the sections above.

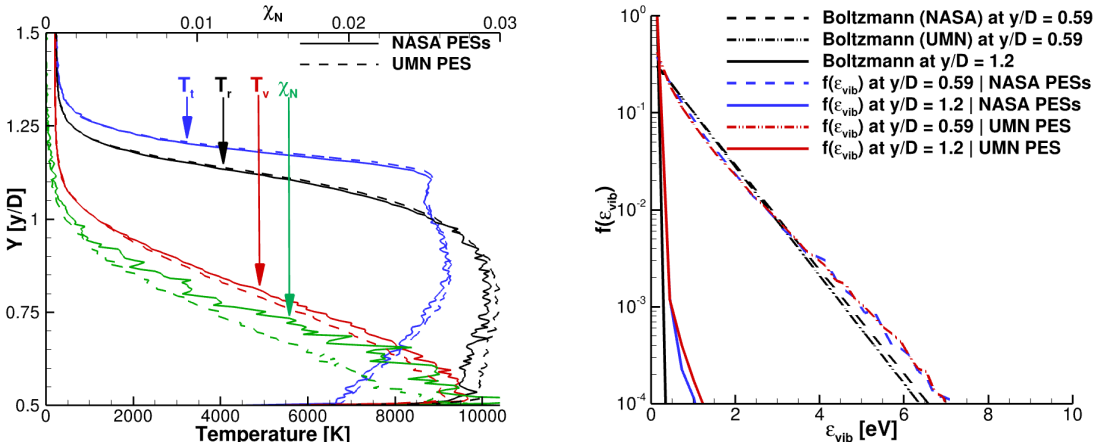


(a) Temperatures and Composition.

(b) Vibrational Distribution Functions.

**Figure 11 Temperature, composition, and vibrational distribution functions along the flank of the cylinder.**

Figure 11(b) shows the vibrational energy distribution at y/D = 0.59 and 1.20. All data corresponding to statistics collected y/D = 1.2 is presented with a solid line. At y/D = 1.2 we notice that the vibrational energy distribution varies slightly from the corresponding Boltzmann distribution, however, this deviation is observed to be less severe than that observed for the vibrational energy distribution, x/D = 1.8 in Fig. 10(b). This is because the weaker oblique shock at the

flank leads to less energetic molecular collisions than the stronger normal shock and, therefore, causes less deviation from Boltzmann behavior.

Figure 11(b) includes two sets of Boltzmann distributions for y/D = 0.59 because $T_v$ = 9000 K when using the NASA PESs, but only 8700 K in the UMN PES. The dashed black curve corresponds to the Boltzmann distribution for $T_v$ = 9000 K and is to be compared with the dashed blue curve showing the vibrational energy distribution obtained from the simulation using the NASA PESs. The DMS predicted solution deviates slightly from the Boltzmann distribution, and exhibits behavior similar to that seen in the near wall distribution of x/D = 2 in Fig. 10(b). The dash-dot black curve shows the Boltzmann distribution for $T_v$ = 8700 K, and is used as a comparison point for for the vibrational energy distribution function obtained from the simulation that uses the UMN PES. It can be seen that both simulations produce similar slightly non-Boltzmann behavior at this location in the flow.

### E. Cylinder Aft

Figure 12(a) shows the temperature and composition profiles in the cylinder wake along the cylinder aft-centerline. We see that the translational temperature (blue) peaks behind the cylinder at about x/D = 3.25, this is where the streamlines close behind the cylinder. As the flow expands behind the cylinder, the translational temperature decreases. The rotational and vibrational modes remain frozen in the cylinder aft. It can be seen that the translational temperature given by the NASA PESs (solid-blue curve) is slightly cooler than the translational temperature given by the UMN PES (solid-blue). Additionally, the rotational (black) and vibrational (blue) temperatures are in equilibrium in the simulation using the NASA PESs (solid curves) behind the shock at $T_r = T_v \sim 9250$ K. Whereas the rotational and vibrational modes are frozen in a nonequilibrium state for the simulation using the UMN PES (dashed curves), with $T_r \sim 9500$ K and $T_v \sim 8700$ K. As such, the NASA PESs simulation results in a slightly higher mass fraction of atomic nitrogen.

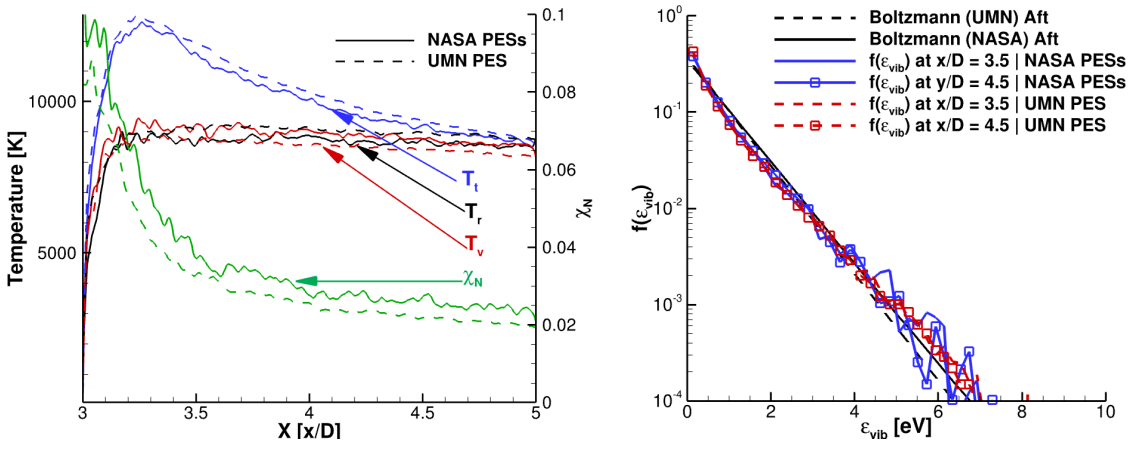


(a) Temperatures and Composition.

(b) Vibrational Distribution Functions.

**Figure 12 Temperature, composition, and vibrational distribution functions along the aft of the cylinder.**

Figure 12(b) shows the vibrational energy distributions given by the simulation using the NASA PESs (solid blue curves) and UMN PES (dashed red curves) at x/D = 3.5 (line) and 4.5 (line with symbols). Additionally, we provide Boltzmann distribution at $T_v$ = 9250 K (solid black line) to compare the NASA PES simulation and at $T_v$ = 8700 K (dashed black line) to compare the UMN PES simulations. The distributions for both simulations do not change between x/D = 3.5 and x/D = 4.5 and are qualitatively similar. Also, these distributions exhibit minor deviation from the corresponding Boltzmann distributions, akin to the non-Boltzmann behavior seen at y/D = 0.59 in Fig. 11(b) and x/D = 2.0 in Fig. 10(b).

## V. Conclusions

In this article we present a comparative atomic level study analyzing the vibrational excitation and dissociation of molecular nitrogen due to $N_2$ ($^1\Sigma_g^+$) + N ($^4S_u$) and $N_2$ ($^1\Sigma_g^+$) + $N_2$ ($^1\Sigma_g^+$) interactions governed by independently developed potential energy surfaces at the University of Minnesota [9, 10] and NASA Ames Research Center [11, 12] at temperatures relevant at hypersonic reentry conditions. Vibrational excitation was studied for $N_2$ + $N_2$ interactions from T = 10000 K to 30000 K and for $N_2$ + N from T = 5000 K to 30000 K. A maximum variation of 16% is found for the predicted characteristic vibrational excitation time constant due to $N_2$ + $N_2$ interactions and 28% for $N_2$ + N interactions, with the difference decreasing with increase in temperature. Furthermore, nonequilibrium dissociation is studied from T = 10000 K to 30000 K under the quasi-steady state (QSS) conditions. It is observed that the two PESs give the same non-Boltzmann distributions in the QSS regime. However, the QSS dissociation rate coefficients were found to differ by 50 % for both $N_2$ + $N_2$ and $N_2$ + N interactions at 10000 K. This difference decreases with increase in temperature.

In addition, an inviscid Mach 20 dissociating nitrogen flow over a cylinder is studied with the DMS method using the two sets of independently developed PESs. This flow is characterized by rotational and vibrational excitation, dissociation, and thermal nonequilibrium throughout the flow field. The simulations using the NASA PESs and the UMN PES are shown to qualitatively predict similar flow features. However, it is observed that the NASA PES allows for slightly faster vibrational excitation, quicker vibrational-rotational equilibration in the flow field. The simulation using the NASA PES also predict a higher fraction of atomic nitrogen in the flow field, with the maximum difference of atomic nitrogen mass fraction being about 28% in the cylinder wake.

It is observed that the vibrational energy distributions have a non-Boltzmann nature during the vibrational excitation in the stagnation region of the flow, with both simulations predicting similar deviation from Boltzmann behavior. Similarly, non-Boltzmann distributions are observed in the expanding flow along the flank and aft of the cylinder, and both simulations provide a similar description of the non-Boltzmann characteristics of the flow field.

In conclusion, independently developed PESs at the University of Minnesota [9, 10] and NASA Ames Research Center [11, 12] for $N_2$ + $N_2$ and $N_2$ + N interactions were used to simulate heat baths and a canonical dissociating hypersonic flow. In these simulations, these interactions on these PESs produce remarkably similar results for

macroscopic and microscopic properties of the flow. Such favorable comparison yields confidence in the use of *ab initio* PESs to obtain thermochemical characteristics of reacting hypersonic flow.

## VI. Acknowledgements

We gratefully acknowledge partial funding by U.S. Air Force Office of Scientific Research (AFOSR) under grant 21RQCOR045. We would like to thank the DoD HPCMP and the Texas Advanced Computing Center (TACC), and the DoE INCITE grant for providing supercomputing resources for this work. R. Jaffe would like to acknowledge NASA Space Technology Directorate Entry Systems Modeling project for support. T. Schwartzentruber acknowledges support of the AFOSR under grant FA 9550-19-1-0219. This article was cleared for public release under case file number AFRL-2022-2823 on 14 June 2022.

## References

[1] Candler, G. V., "Rate Effects in Hypersonic Flows," *Annual Review of Fluid Mechanics*, Vol. 51, 2018, p. 2019.

[2] Park, C., "Assessment of a two-temperature kinetic model for dissociating and weakly ionizing nitrogen," *Journal of Thermophysics and Heat Transfer*, Vol. 2, No. 1, 1988, pp. 8–16.

[3] Park, C., "Review of chemical-kinetic problems of future NASA missions, I: Earth entries," *Journal of Thermophysics and Heat Transfer*, Vol. 7, No. 3, 1993, pp. 385–398.

[4] Park, C., Howe, J. T., Jaffe, R. L., and Candler, G. V., "Review of chemical-kinetic problems of future NASA missions, II: Mars entries," *Journal of Thermophysics and Heat Transfer*, Vol. 8, No. 1, 1994, pp. 9–23.

[5] Byron, S., "Shock-Tube Measurement of the Rate of Dissociation of Nitrogen," *The Journal of Chemical Physics*, Vol. 44, No. 4, 1966, pp. 1378–1388.

[6] Kewley, D. J., and Hornung, H. G., "Free-piston shock-tube study of nitrogen dissociation," *Chemical Physics Letters*, Vol. 25, No. 4, 1974, pp. 531–536.

[7] Appleton, J. P., Steinberg, M., and Liquornik, D. J., "Shock-Tube Study of Nitrogen Dissociation using Vacuum-Ultraviolet Light Absorption," *The Journal of Chemical Physics*, Vol. 48, No. 2, 1968, pp. 599–608.

[8] Hanson, R. K., and Baganoff, D., "Shock-tube study of nitrogen dissociation rates using pressure measurements," *AIAA Journal*, Vol. 10, No. 2, 1972, pp. 211–215.

[9] Paukku, Y., Yang, K. R., Varga, Z., and Truhlar, D. G., "Global ab initio ground-state potential energy surface of N4," *The Journal of chemical physics*, Vol. 139, No. 4, 2013, p. 044309.

[10] Bender, J. D., Valentini, P., Nompelis, I., Paukku, Y., Varga, Z., Truhlar, D. G., Schwartzentruber, T. E., and Candler, G. V., "An improved potential energy surface and multi-temperature quasiclassical trajectory calculations of N2+ N2 dissociation reactions," *The Journal of chemical physics*, Vol. 143, No. 5, 2015, p. 054304.

[11] Chaban, G., Jaffe, R., Schwenke, D. W., and Huo, W., "Dissociation cross sections and rate coefficients for nitrogen from accurate theoretical calculations," *AIAA paper*, Vol. 1209, 2008, p. 2008.

[12] Jaffe, R., Schwenke, D., and Chaban, G., "Vibrational and rotational excitation and dissociation in N2-N2 collisions from accurate theoretical calculations," *10th AIAA/ASME Joint Thermophysics and Heat Transfer Conference*, Vol. 4517, 2010.

[13] Varga, Z., Paukku, Y., and Truhlar, D. G., "Potential energy surfaces for O+ O2 collisions," *The Journal of chemical physics*, Vol. 147, No. 15, 2017, p. 154312.

[14] Paukku, Y., Yang, K. R., Varga, Z., Song, G., Bender, J. D., and Truhlar, D. G., "Potential energy surfaces of quintet and singlet O4," *The Journal of chemical physics*, Vol. 147, No. 3, 2017, p. 034301.

[15] Paukku, Y., Varga, Z., and Truhlar, D. G., "Potential energy surface of triplet O4," *The Journal of chemical physics*, Vol. 148, No. 12, 2018, p. 124314.

[16] Valentini, P., Grover, M. S., and Josyula, E., "Constructing feed-forward artificial neural networks to fit potential energy surfaces for molecular simulation of high-temperature gas flows," *Physical Review E*, Vol. 102, No. 5, 2020, p. 053302.

[17] Varga, Z., Liu, Y., Li, J., Paukku, Y., Guo, H., and Truhlar, D. G., "Potential energy surfaces for high-energy N+ O2 collisions," *The Journal of Chemical Physics*, Vol. 154, No. 8, 2021, p. 084304.

[18] Truhlar, D. G., and Muckerman, J. T., *Atom-Molecule Collision Theory: A Guide for the Experimentalist*, Plenum Press, New York, NY, 1979.

[19] Billing, G. D., and Fisher, E., "VV and VT rate coefficients in N2 by a quantum-classical model," *Chemical Physics*, Vol. 43, No. 3, 1979, pp. 395–401.

[20] Fernández-Ramos, A., Miller, J. A., Klippenstein, S. J., and Truhlar, D. G., "Modeling the kinetics of bimolecular reactions," *Chemical reviews*, Vol. 106, No. 11, 2006, pp. 4518–4584.

[21] Capitelli, M., Ferreira, C. M., Gordiets, B. F., and Osipov, A. I., *Plasma kinetics in atmospheric gases*, Vol. 31, Springer Science & Business Media, 2013.

[22] Colonna, G., Pietanza, L. D., and Capitelli, M., "Recombination-assisted nitrogen dissociation rates under nonequilibrium conditions," *Journal of Thermophysics and Heat Transfer*, Vol. 22, No. 3, 2008, pp. 399–406.

[23] Munafò, A., Lani, A., Bultel, A., and Panesi, M., "Modeling of non-equilibrium phenomena in expanding flows by means of a collisional-radiative model," *Physics of Plasmas*, Vol. 20, No. 7, 2013, p. 073501.

[24] Kim, J. G., and Boyd, I. D., "Monte Carlo simulation of nitrogen dissociation based on state-resolved cross sections," *Physics of Fluids*, Vol. 26, No. 1, 2014, p. 012006.

[25] Josyula, E., and Bailey, W. F., "Vibration-dissociation coupling using master equations in nonequilibrium hypersonic blunt-body flow," *Journal of thermophysics and heat transfer*, Vol. 15, No. 2, 2001, pp. 157–167.

[26] Sahai, A., Lopez, B., Johnston, C., and Panesi, M., "Adaptive coarse graining method for energy transfer and dissociation kinetics of polyatomic species," *The Journal of Chemical Physics*, Vol. 147, No. 5, 2017, p. 054107.

[27] Macdonald, R., Jaffe, R., Schwenke, D., and Panesi, M., "Construction of a coarse-grain quasi-classical trajectory method. I. Theory and application to N2–N2 system," *The Journal of chemical physics*, Vol. 148, No. 5, 2018, p. 054309.

[28] Panesi, M., Jaffe, R. L., Schwenke, D. W., and Magin, T. E., "Rovibrational internal energy transfer and dissociation of N 2 (1 Σ g+)- N (4 S u) system in hypersonic flows," *The Journal of chemical physics*, Vol. 138, No. 4, 2013, p. 044312.

[29] Andrienko, D. A., and Boyd, I. D., "Rovibrational energy transfer and dissociation in O2–O collisions," *The Journal of chemical physics*, Vol. 144, No. 10, 2016, p. 104301.

[30] Liu, Y., Vinokur, M., Panesi, M., and Magin, T., "A multi-group maximum entropy model for thermo-chemical nonequilibrium," *AIAA paper*, Vol. 4332, 2010, p. 2010.

[31] Panesi, M., and Lani, A., "Collisional radiative coarse-grain model for ionization in air," *Physics of Fluids*, Vol. 25, No. 5, 2013, p. 057101.

[32] Kustova, E. V., and Nagnibeda, E. A., "Kinetic model for multi-temperature flows of reacting carbon dioxide mixture," *Chemical Physics*, Vol. 398, 2012, pp. 111–117.

[33] Macdonald, R., Grover, M., Schwartzentruber, T., and Panesi, M., "Construction of a coarse-grain quasi-classical trajectory method. II. Comparison against the direct molecular simulation method," *The Journal of chemical physics*, Vol. 148, No. 5, 2018, p. 054310.

[34] Schwartzentruber, T. E., Grover, M. S., and Valentini, P., "Direct molecular simulation of nonequilibrium dilute gases," *Journal of Thermophysics and Heat Transfer*, Vol. 32, No. 4, 2018, pp. 892–903.

[35] Valentini, P., Schwartzentruber, T. E., Bender, J. D., Nompelis, I., and Candler, G. V., "Direct molecular simulation of nitrogen dissociation based on an ab initio potential energy surface," *Physics of Fluids*, Vol. 27, No. 8, 2015, p. 086102.

[36] Valentini, P., Schwartzentruber, T. E., Bender, J. D., and Candler, G. V., "Dynamics of nitrogen dissociation from direct molecular simulation," *Physical Review Fluids*, Vol. 1, No. 4, 2016, p. 043402.

[37] Torres, E., and Schwartzentruber, T. E., "Direct molecular simulation of dissociating nitrogen in an adiabatic reactor," *AIAA Scitech 2019 Forum*, 2019, p. 1049.

[38] Grover, M. S., Schwartzentruber, T. E., Varga, Z., and Truhlar, D. G., "Dynamics of vibrational energy excitation and dissociation in oxygen from direct molecular simulation," *2018 AIAA Aerospace Sciences Meeting*, 2018, p. 0238.

[39] Grover, M. S., Torres, E., and Schwartzentruber, T. E., "Direct molecular simulation of internal energy relaxation and dissociation in oxygen," *Physics of Fluids*, Vol. 31, No. 7, 2019, p. 076107.

[40] Torres, E., and Schwartzentruber, T. E., "Direct molecular simulation of oxygen dissociation across normal shocks," *Theoretical and Computational Fluid Dynamics*, 2022, pp. 1–40.

[41] Grover, M. S., and Valentini, P., "Ab initio simulation of hypersonic flows past a cylinder based on accurate potential energy surfaces," *Physics of Fluids*, 2021, p. [Accepted].

[42] Valentini, P., Grover, M. S., Bisek, N., and Verhoff, A., "Molecular simulation of flows in thermochemical non-equilibrium around a cylinder using ab initio potential energy surfaces for N2+ N and N2+ N2 interactions," *Physics of Fluids*, Vol. 33, No. 9, 2021, p. 096108.

[43] Grover, M. S., Valentini, P., Bisek, N. J., and Verhoff, A. M., "Ab initio simulation of a dissociating nitrogen flow over a wedge," *AIAA SCITECH 2022 Forum*, 2022, p. 0873.

[44] Valentini, P., Grover, M. S., Bisek, N. J., and Verhoff, A. M., "Viscosity of nitrogen from ab initio direct molecular simulations," *AIAA SCITECH 2022 Forum*, 2022, p. 0875.

[45] Bird, G. A., *Molecular Gas Dynamics and Simulation of Gas Flows*, Cambridge University Press, Cambridge, England, 1994.

[46] Frenkel, D., and Smit, B., *Understanding Molecular Simulation: From Algorithms to Applications*, Academic Press, San Diego, CA, 2002.

[47] Geistfeld, E. C., Torres, E., and Schwartzentruber, T. E., "Quasi Classical Trajectory Analysis of Oxygen Recombination Using a Consistent Binary Lifetime Framework," *AIAA SCITECH 2022 Forum*, 2022, p. 1635.

[48] Kondur, C., and Stephani, K. A., "Rate constants and molecular recombination pathways of oxygen from quasi-classical trajectory simulations of the O3 system," *Chemical Physics*, Vol. 552, 2022, p. 111357.

[49] Plimpton, S., Moore, S., Borner, A., Stagg, A., Koehler, T., Torczynski, J., and Gallis, M., "Direct simulation Monte Carlo on petaflop supercomputers and beyond," *Physics of Fluids*, Vol. 31, No. 8, 2019, p. 086101. `http://sparta.sandia.govs`.

[50] Ling, M. S. H., and Rigby, M., "Towards an intermolecular potential for nitrogen," *Molecular Physics*, Vol. 51, No. 4, 1984, pp. 855–882.

[51] Eyring, H., and Polanyi, M., "Uber einfache gasreaktionen," *Z Phys Chem Abt B*, Vol. 12, 1931, pp. 279–311.

[52] London, P., "Sommerfeld Festschrift (1928)," *Z. Electrochemie*, Vol. 35, 1929, p. 552.

[53] Sato, S., "On a new method of drawing the potential energy surface," *The Journal of chemical physics*, Vol. 23, No. 3, 1955, pp. 592–593.

[54] Sato, S., "Potential energy surface of the system of three atoms," *The Journal of Chemical Physics*, Vol. 23, No. 12, 1955, pp. 2465–2466.

[55] Karplus, M., Porter, R. N., and Sharma, R. D., "Exchange reactions with activation energy. I. Simple barrier potential for (H, H2)," *The Journal of Chemical Physics*, Vol. 43, No. 9, 1965, pp. 3259–3287.

[56] Jaffe, R. L., Schwenke, D. W., Grover, M., Valentini, P., Schwartzentruber, T. E., Venturi, S., and Panesi, M., "Comparison of quantum mechanical and empirical potential energy surfaces and computed rate coefficients for N2 dissociation," *54th AIAA Aerospace Sciences Meeting*, 2016, p. 0503.

[57] Dunning Jr, T. H., "Gaussian basis sets for use in correlated molecular calculations. I. The atoms boron through neon and hydrogen," *The Journal of chemical physics*, Vol. 90, No. 2, 1989, pp. 1007–1023.

[58] Kendall, R. A., Dunning Jr, T. H., and Harrison, R. J., "Electron affinities of the first-row atoms revisited. Systematic basis sets and wave functions," *The Journal of chemical physics*, Vol. 96, No. 9, 1992, pp. 6796–6806.

[59] Purvis III, G. D., and Bartlett, R. J., "A full coupled-cluster singles and doubles model: The inclusion of disconnected triples," *The Journal of Chemical Physics*, Vol. 76, No. 4, 1982, pp. 1910–1918.

[60] Gdanitz, R. J., and Ahlrichs, R., "The averaged coupled-pair functional (ACPF): A size-extensive modification of MR CI (SD)," *Chemical physics letters*, Vol. 143, No. 5, 1988, pp. 413–420.

[61] Roos, B. O., Taylor, P. R., Si, P. E. M., et al., "A complete active space SCF method (CASSCF) using a density matrix formulated super-CI approach," *Chemical Physics*, Vol. 48, No. 2, 1980, pp. 157–173.

[62] Le Roy, R. J., Huang, Y., and Jary, C., "An accurate analytic potential function for ground-state N 2 from a direct-potential-fit analysis of spectroscopic data," *The Journal of chemical physics*, Vol. 125, No. 16, 2006, p. 164310.

[63] Papajak, E., Leverentz, H. R., Zheng, J., and Truhlar, D. G., "Efficient Diffuse Basis Sets: cc-pV x Z+ and maug-cc-pV x Z," *Journal of chemical theory and computation*, Vol. 5, No. 5, 2009, pp. 1197–1202.

[64] Andersson, K., Malmqvist, P., and Roos, B. O., "Second-order perturbation theory with a complete active space self-consistent field reference function," *The Journal of chemical physics*, Vol. 96, No. 2, 1992, pp. 1218–1226.

[65] Werner, H. J., "Third-order multireference perturbation theory The CASPT3 method," *Molecular Physics*, Vol. 89, No. 2, 1996, pp. 645–661.

[66] Finley, J., Malmqvist, P., Roos, B. O., and Serrano-Andrés, L., "The multi-state CASPT2 method," *Chemical physics letters*, Vol. 288, No. 2-4, 1998, pp. 299–306.

[67] Jaffe, R. L., "The calculation of high-temperature equilibrium and nonequilibrium specific heat data for N2, O2 and NO," *22nd Thermophysics Conference*, 1987, p. 1633.

[68] Grover, M. S., "Direct Molecular Simulation of Nitrogen and Oxygen at Hypersonic Conditions," Ph.D. thesis, University of Minnesota, Minnesota, MN, 2018.

[69] Millikan, R. C., and White, D. R., "Systematics of vibrational relaxation," *The Journal of chemical physics*, Vol. 39, No. 12, 1963, pp. 3209–3213.

[70] Macdonald, R. L., Torres, E., Schwartzentruber, T. E., and Panesi, M., "State-to-state master equation and direct molecular simulation study of energy transfer and dissociation for the N2–N system," *The Journal of Physical Chemistry A*, Vol. 124, No. 35, 2020, pp. 6986–7000.

[71] Chaudhry, R. S., and Candler, G. V., "Statistical Analyses of Quasiclassical Trajectory Data for Air Dissociation," *AIAA Scitech 2019 Forum*, 2019, p. 0789.

[72] Singh, N., and Schwartzentruber, T., "Consistent kinetic–continuum dissociation model I. Kinetic formulation," *The Journal of chemical physics*, Vol. 152, No. 22, 2020, p. 224302.

[73] Li, J., Varga, Z., Truhlar, D. G., and Guo, H., "Many-body permutationally invariant polynomial neural network potential energy surface for N4," *Journal of Chemical Theory and Computation*, Vol. 16, No. 8, 2020, pp. 4822–4832.